

Electronic Supplementary Information

Built-in Superionic Conductive Phases Enabling Dendrite-free, Long Lifespan and High Specific Capacity of Composite Lithium for Stable Solid-State Lithium Batteries

Guanjie Lu^a, Menghong Li^a, Peng Chen^e, Weikang Zheng^b, Zuguang Yang^a, Ronghua Wang^{b,*}, and Chaohe Xu^{a,c,d,*}

^a College of Aerospace Engineering, Chongqing University, Chongqing, 400044, China

^b College of Materials Science and Engineering, Chongqing University, Chongqing, 400044, China

^c National Engineering Research Center for Magnesium Alloys, Chongqing University, Chongqing, 400044, China

^d State Key Laboratory of Power Transmission Equipment & System Security and New Technology, Chongqing University, Chongqing, 400044, China

^e Institute for Innovative Materials and Energy, Faculty of Chemistry and Chemical Engineering, Yangzhou University, Yangzhou City, Jiangsu Province, 225009, China

Email: xche@cqu.edu.cn (C. Xu) ; wangrh@cqu.edu.cn (R. Wang)

1. Supplementary Figures

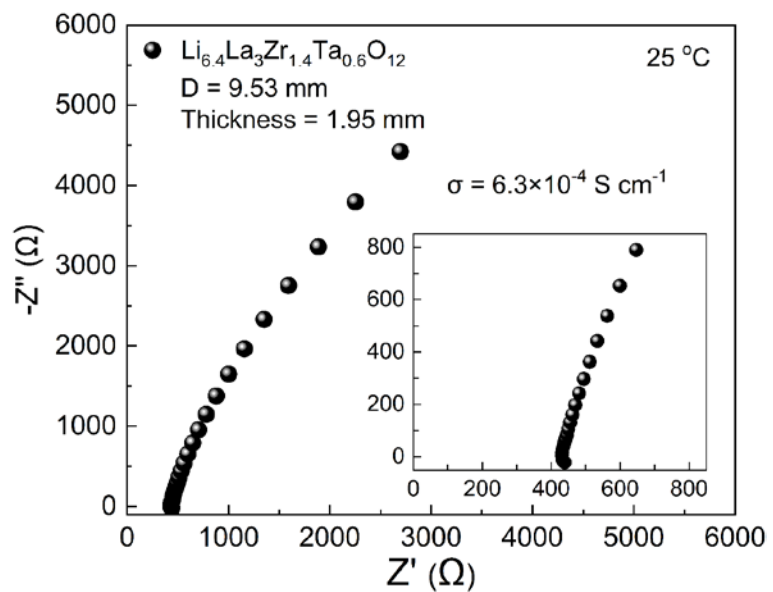


Figure S1. EIS plot of the as-synthesized LLZTO electrolyte with Pt as the Li^+ blocking electrodes at $25 \text{ }^\circ\text{C}$. The inset is the enlarged curve at high frequency zone.

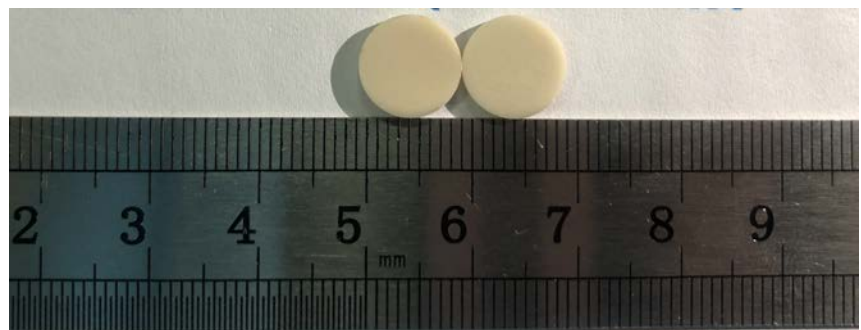


Figure S2. Digital photo of the as-synthesized LLZTO pellets.

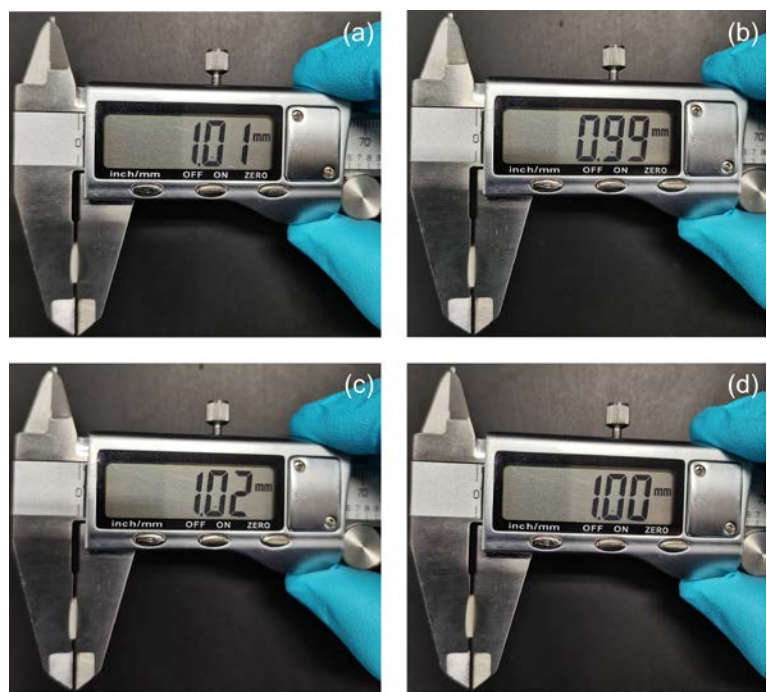


Figure S3. The thickness of the LLZTO-based SEs after polishing.

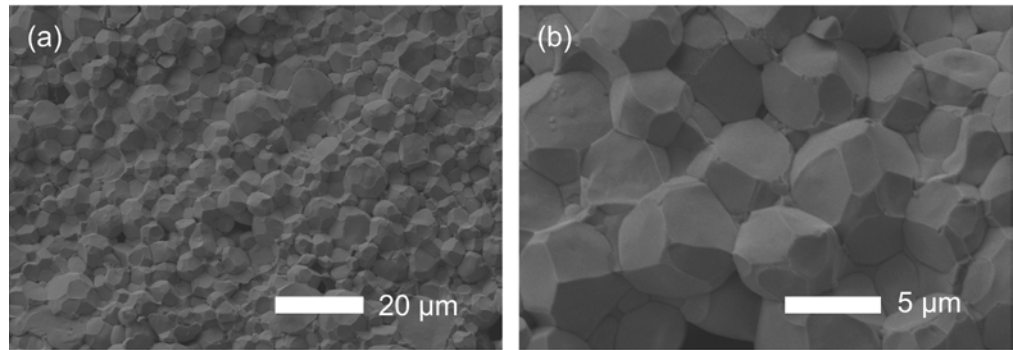


Figure S4. Cross-section SEM images of the LLZTO electrolyte at different magnifications. The relative density is determined to be ~95%.

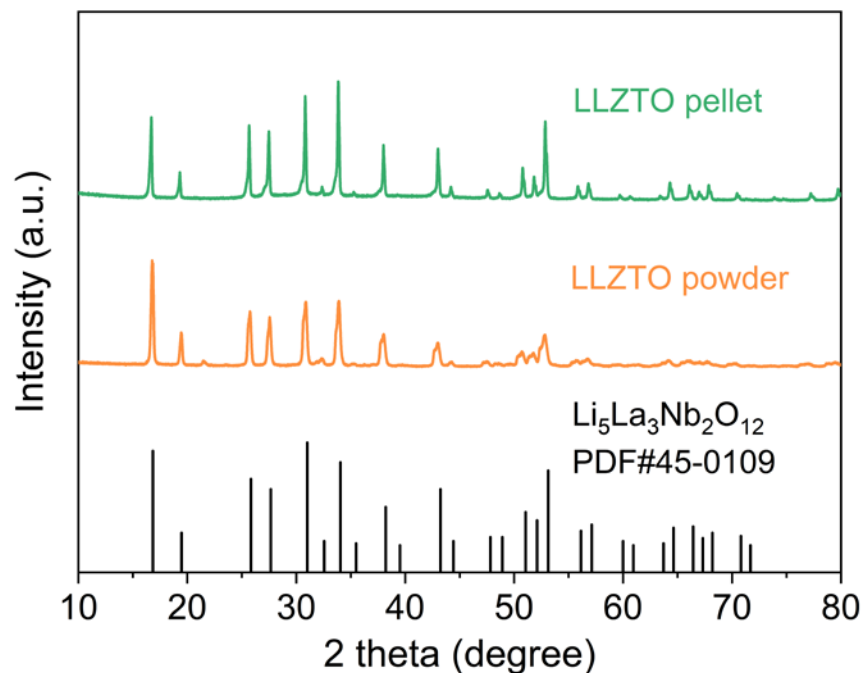


Figure S5. XRD patterns of the as-synthesized garnet solid electrolyte powders and pellet.

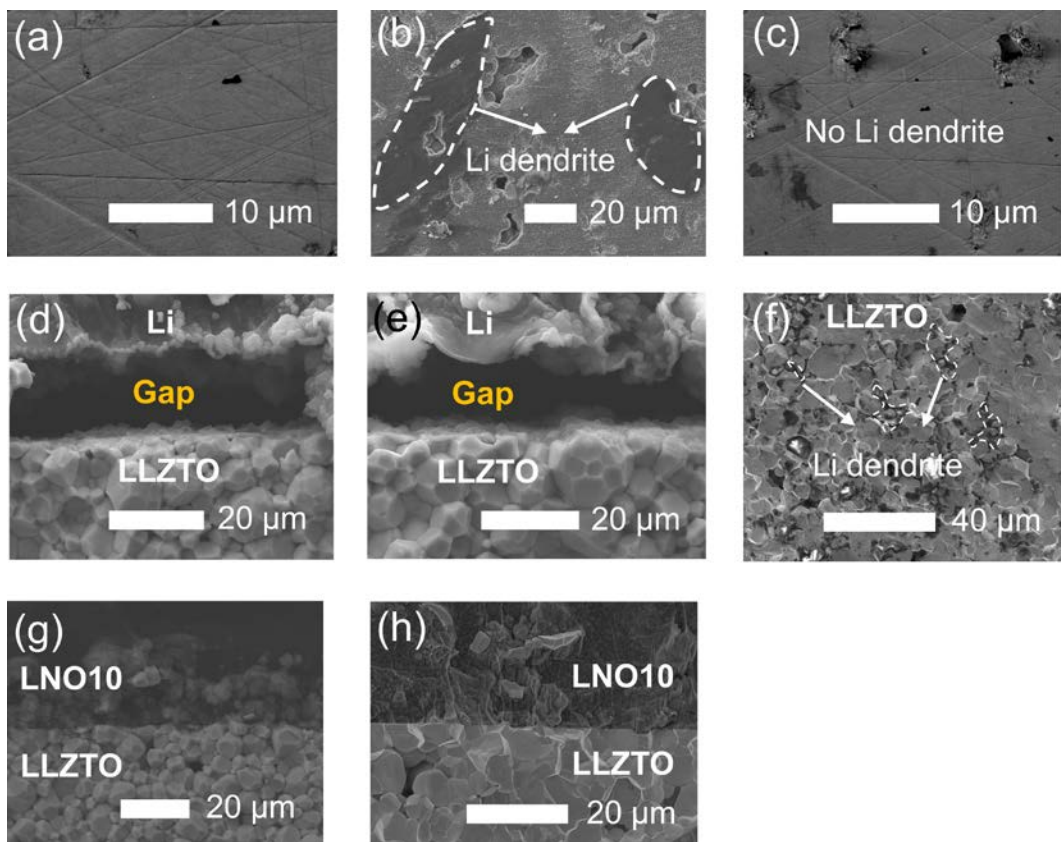


Figure S6. Morphology evolutions of surface and cross-section image for the bare Li and composite Li. (a) The surface morphologies of the LLZTO pellet before cycling. The surface morphologies of the LLZTO pellet after cycling for the bare Li (b) and composite Li (c). Cross-section SEM images of the bare Li before (d) and after cycling (e). (f) Cross-section SEM images of the LLZTO after cycling. Cross-section SEM images of the composite Li before (g) and after cycling (h).

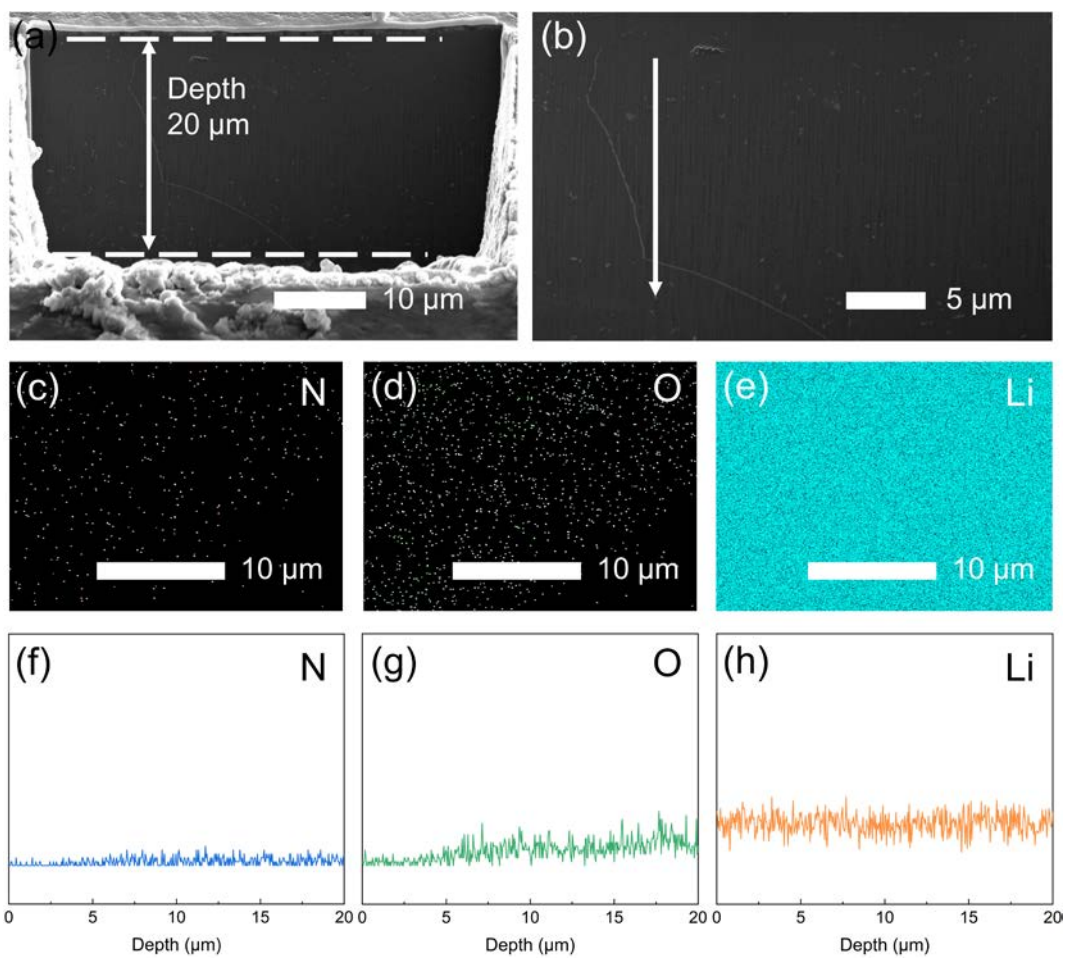


Figure S7. (a-b) Cross-section FIB-SEM images of LNO composite anode. (c-e) The cross-section EDS mapping images of LNO composite anode. (f-h) Elemental line scanning of N, O and Li.

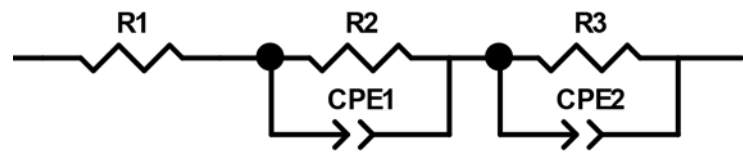


Figure S8. Equivalent circuit for modeling the impedance spectra of LNO10/LLZTO/LNO10 and Li/ LLZTO/Li symmetric cells.

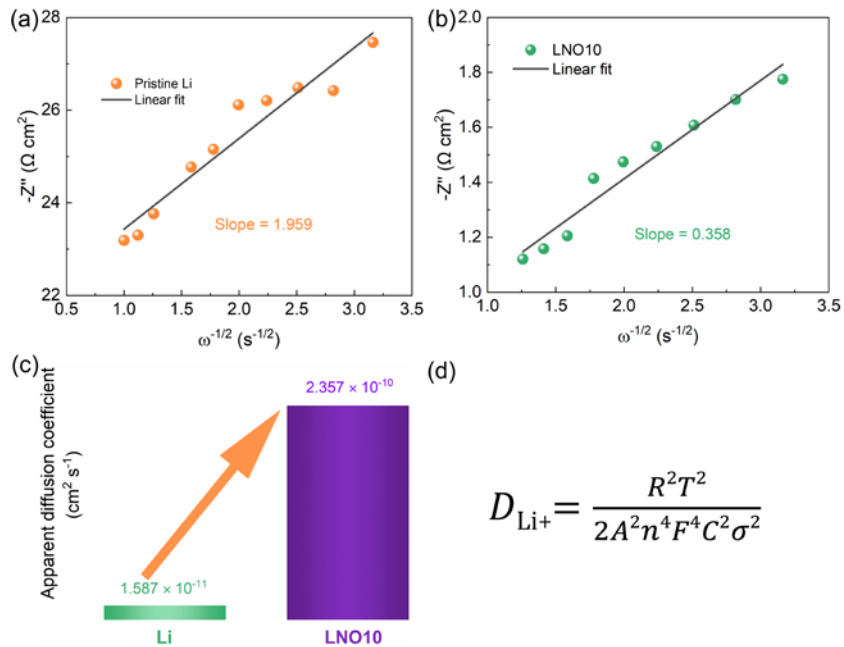


Figure S9. Warburg coefficient of the a) pristine Li cell, b) LNO10 cell, and c) the corresponding calculated Li^+ apparent diffusion coefficient. (d) Computational formula of lithium-ion diffusion coefficients (D_{Li^+})

Fitting the low-frequency region of the impedance spectrum in **Figure 4c**, the Warburg coefficient can be calculated from the slope of the low-frequency region, and then the Li^+ apparent diffusion coefficient can be obtained according to the formula in **Figure S9d**. For the computational formula of **Figure S9d**, R is the gas constant, T is the absolute temperature, A is the surface area of the electrode, n is the number of electrons per molecule during oxidation, F is the Faraday constant, and C is the concentration of lithium ions.

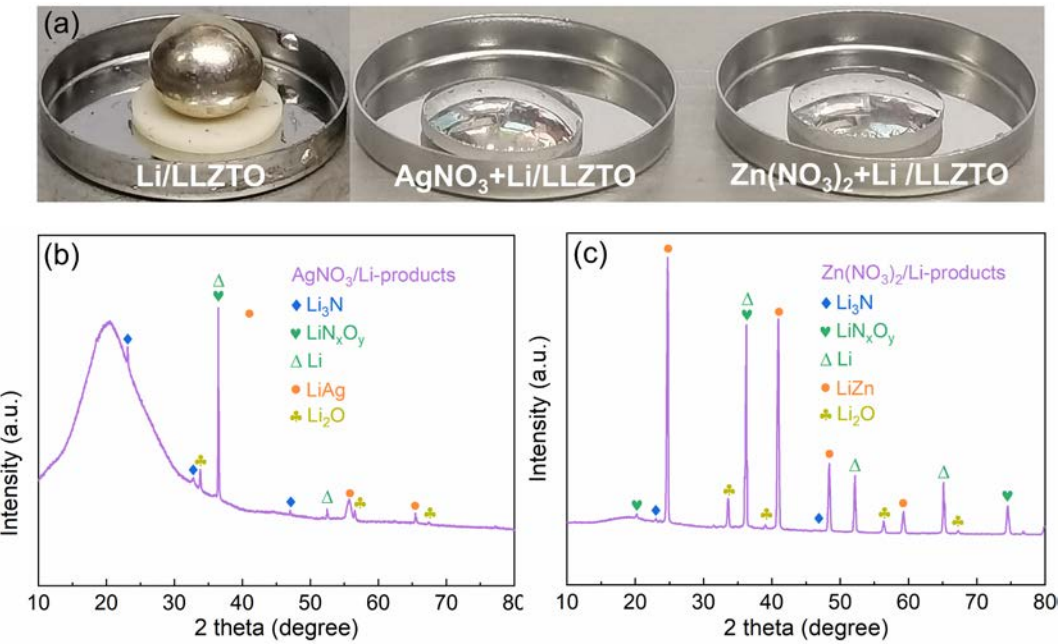


Figure S10. (a) Digital photos of the wetting behaviors of molten Li with the LLZTO SSEs, Li-AgNO₃ composite electrodes with 10 wt% AgNO₃ with the LLZTO SSEs, and Li-Zn(NO₃)₂ composite electrodes with 10 wt% Zn(NO₃)₂ with the LLZTO SSEs, respectively. (b) XRD pattern of the products obtained by reaction of AgNO₃ power and molten lithium. (c) XRD pattern of the products obtained by reaction of Zn(NO₃)₂ power and molten lithium.

Note: In the case of AgNO₃, Li₃N, LiN_xO_y, LiAg alloy and excess Li could be observed after reacting with molten Li, as exhibited in **Figure S10b**. When comes to Zn(NO₃)₂, there are Li₃N, LiN_xO_y, LiZn alloy and excess Li in the final product (**Figure S10c**).

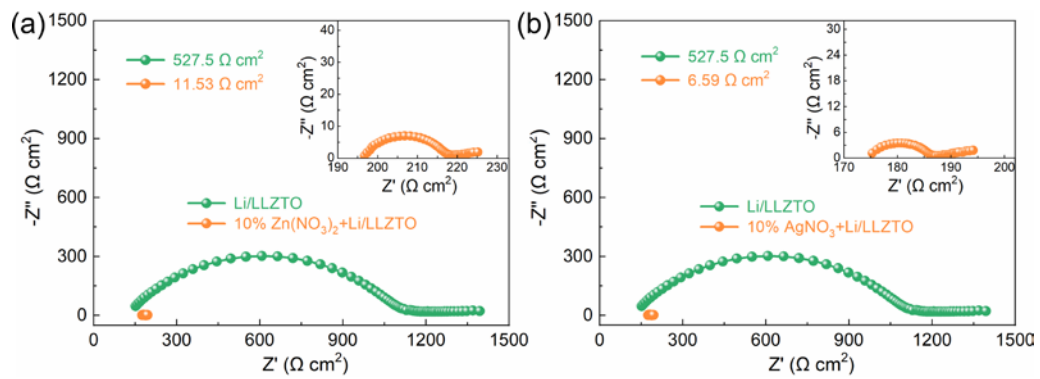


Figure S11. (a) Nyquist plots of symmetric cells with pure Li and Li-Zn(NO_3)₂ composite electrodes with 10 wt% Zn(NO_3)₂. (b) Nyquist plots of symmetric cells with pure Li and Li-AgNO₃ composite electrodes with 10 wt% AgNO₃.

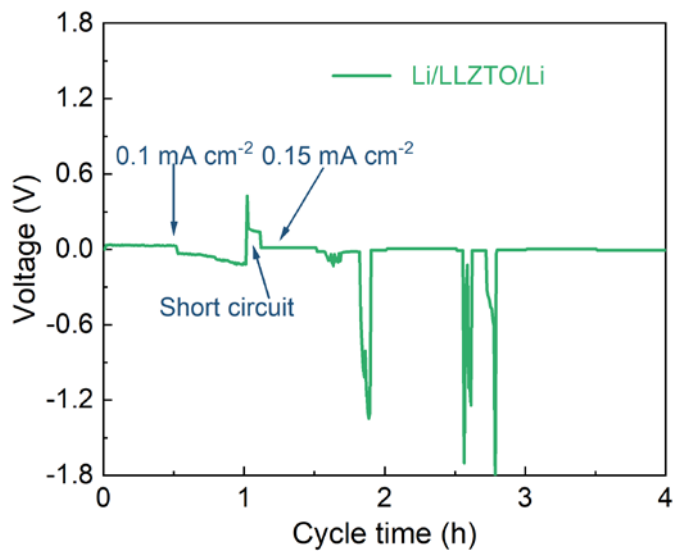


Figure S12. Galvanostatic cycling of the symmetric Li cells with pristine LLZTO electrolyte at 0.1 and 0.15 mA cm⁻².

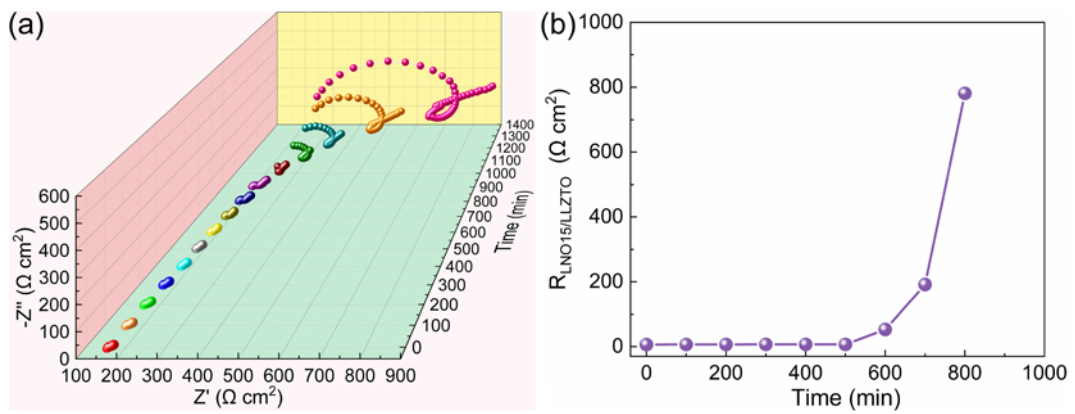


Figure S13. (a) GEIS of the LNO15/LLZTO/LNO15 symmetric cells under 0.1 mA cm^{-2} at RT. (b) The interface impedance contributions obtained from the analysis of the LNO15/LLZTO/LNO15 symmetric cells impedance spectra.

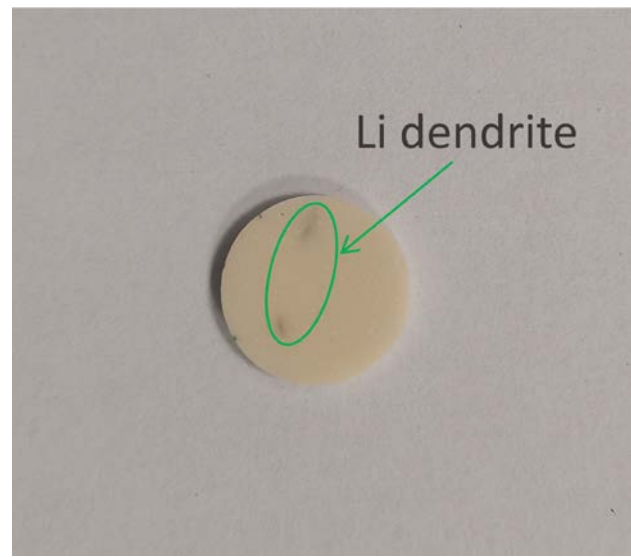


Figure S14. Optical image of the LLZTO pellet after short circuit.

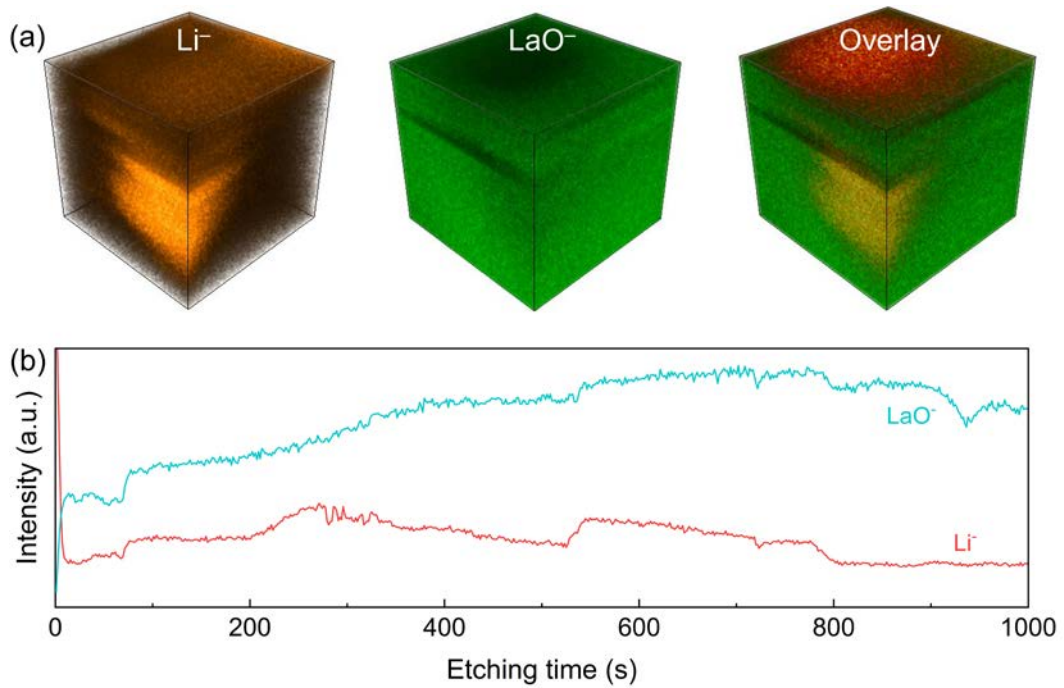


Figure S15. (a) TOF-SIMS 3D illustration of Li^- , LaO^- , and overlay along the depth. These signals are collected from the cycled LLZTO electrolyte by TOF-SIMS. (b) TOF-SIMS depth profiles of cycled LLZTO electrolyte. Li^- , LaO^- , and overlay were used as representative species for profiling.

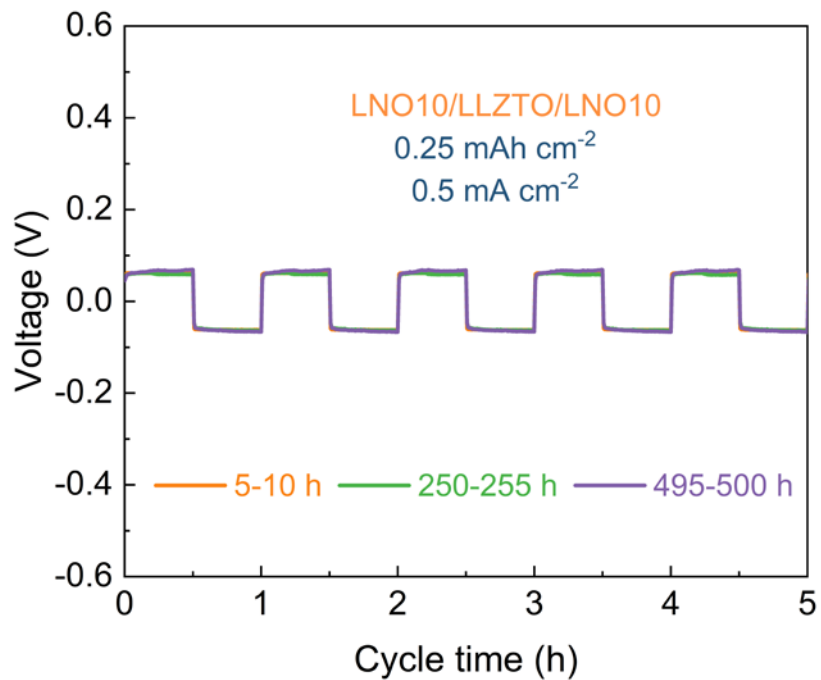


Figure S16. The enlarged long-term galvanostatic cycles of the symmetric LNO10/LLZTO/LNO10 cell at 0.5 mA cm^{-2} from 5 to 10 h, 250 to 255 h, and 495 to 500 h, respectively.

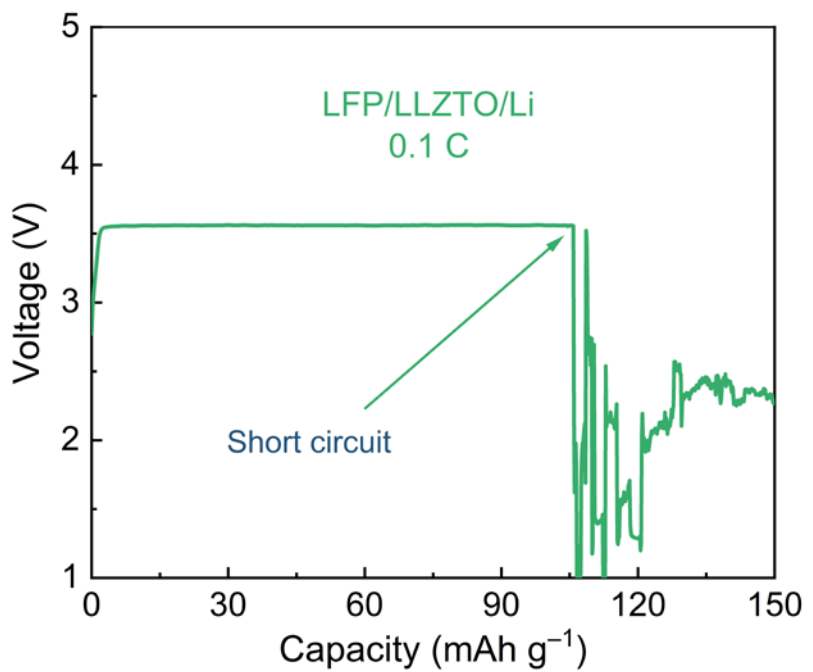


Figure S17. Charge/discharge curves of the semi-solid LFP/LE-LLZTO/Li batteries with a pristine LLZTO pellet under 0.1 C.

Table S1. Critical current density (CCD), area specific resistance (ASR) and cycling stability of the reported Li-Li symmetrical batteries using garnet solid-state electrolytes with different interfacial layers.

Solid electrolyte	Interfacial layer	ASR ($\Omega \text{ cm}^2$)	CCD (mA cm^{-2})	Stability ($\text{mA cm}^{-2}/\text{h}$)	Ref.
$\text{Li}_7\text{La}_{2.75}\text{Ca}_{0.25}\text{Zr}_{1.75}\text{Nb}_{0.25}\text{O}_{12}$	Vapor Deposition	75 (25 °C)	N/A	0.2/42	1
	Method/Al	30 (60 °C)			
$\text{Li}_7\text{La}_{2.75}\text{Ca}_{0.25}\text{Zr}_{1.75}\text{Nb}_{0.25}\text{O}_{12}$	ALD/ZnO	100	N/A	0.1/48	2
$\text{Li}_{6.6}\text{La}_3\text{Zr}_{1.6}\text{Ta}_{0.4}\text{O}_{12}$	MS/Au	140 (25 °C)	0.8 (50 °C)	0.08/150 (25 °C)	3
			0.5 (25 °C)	0.25/150 (50 °C)	
$\text{Li}_{6.85}\text{La}_{2.9}\text{Ca}_{0.1}\text{Zr}_{1.75}\text{Nb}_{0.25}\text{O}_{12}$	PECVD/Si	127	0.2	0.1/225	4
$\text{Li}_{6.5}\text{La}_3\text{Zr}_{1.5}\text{Ta}_{0.5}\text{O}_{12}$	PECVD/Li ₃ N	175 (25 °C)	N/A	0.1/210 (25 °C)	5
$\text{Li}_7\text{La}_{2.75}\text{Ca}_{0.25}\text{Zr}_{1.75}\text{Nb}_{0.25}\text{O}_{12}$	ALD/Al ₂ O ₃	34 (RT)	0.2	0.2/90 (RT)	6
$\text{Li}_{6.5}\text{La}_3\text{Zr}_{1.5}\text{Ta}_{0.5}\text{O}_{12}$	Li-C	11 (RT)	1.0 (RT)	0.3/250 (RT)	7
$\text{Li}_{6.4}\text{La}_3\text{Zr}_{1.4}\text{Ta}_{0.6}\text{O}_{12}$	Acid (HCl-H ₂ SO ₄)	26 (30 °C)	N/A	0.2/700 (30 °C)	8
$\text{Li}_{6.4}\text{La}_3\text{Zr}_{1.4}\text{Ta}_{0.6}\text{O}_{12}$	MS/Cu ₃ N	41.7 (25 °C)	1.2 (25 °C)	0.1/1000 (25 °C)	9
$\text{Li}_{6.85}\text{La}_{2.9}\text{Ca}_{0.1}\text{Zr}_{1.75}\text{Nb}_{0.25}\text{O}_{12}$	Ge	115 (RT)	N/A	0.05/160 (RT)	10
$\text{Li}_{6.5}\text{La}_3\text{Zr}_{1.5}\text{Ta}_{0.5}\text{O}_{12}$	Li-Al alloy	<1 (25 °C)	0.9 (25 °C) 2.3 (60 °C)	0.2/3000 (25 °C)	11
$\text{Li}_{6.5}\text{La}_3\text{Zr}_{1.5}\text{Ta}_{0.5}\text{O}_{12}$	C Reduction	28 (25 °C) 9 (65 °C)	N/A	0.1/450 (25 °C)	12
$\text{Li}_7\text{La}_{2.75}\text{Ca}_{0.25}\text{Zr}_{1.75}\text{Nb}_{0.25}\text{O}_{12}$	MS/Mg	70 (RT)	N/A	0.1/37 (RT)	13
$\text{Li}_{6.375}\text{La}_3\text{Zr}_{1.375}\text{Nb}_{0.625}\text{O}_{12}$	MS/Sn	46.6 (RT)	N/A	0.5/500 (RT)	14
$\text{Li}_7\text{La}_{2.75}\text{Ca}_{0.25}\text{Zr}_{1.75}\text{Nb}_{0.25}\text{O}_{12}$	MS/Ag	66	N/A	0.2/100	15
$\text{Li}_7\text{La}_{2.75}\text{Ca}_{0.25}\text{Zr}_{1.75}\text{Nb}_{0.25}\text{O}_{12}$	MS/Cu ₆ Sn ₅	236	N/A	0.25/300	16
$\text{Li}_{6.4}\text{La}_3\text{Zr}_{1.4}\text{Ta}_{0.6}\text{O}_{12}$	PEO-PAS	200 (65 °C)	0.5 (65 °C)	0.5/10 (65 °C)	17
$\text{Li}_{5.9}\text{Al}_{0.2}\text{La}_3\text{Zr}_{1.75}\text{W}_{0.25}\text{O}_{12}$	Drawing Soft Graphite	13 (RT)	N/A	0.3/1003 (RT)	18
$\text{Li}_{6.5}\text{La}_3\text{Zr}_{1.5}\text{Ta}_{0.5}\text{O}_{12}$	Polishing MoS ₂	7 (100 °C)	2.2 (100 °C)	0.8/240 (100 °C)	19
$\text{Li}_{6.5}\text{La}_3\text{Zr}_{1.5}\text{Ta}_{0.5}\text{O}_{12}$	Li-gC ₃ N ₄	11 (RT)	1.5 (RT)	0.3/300 (RT)	20
$\text{Li}_{6.5}\text{La}_3\text{Zr}_{1.5}\text{Ta}_{0.5}\text{O}_{12}$	Painting/Ga	19.5 (RT) 5 (60 °C)	1.7 (RT)	0.2/2000 (RT)	21
				0.2/9930 (60 °C) 1/150 (60 °C)	
$\text{Li}_{6.5}\text{La}_3\text{Zr}_{1.5}\text{Ta}_{0.5}\text{O}_{12}$	Li-BN	9 (RT)	1.5 (RT)	0.3/380 (RT)	22
$\text{Li}_{6.4}\text{La}_3\text{Zr}_{1.4}\text{Ta}_{0.6}\text{O}_{12}$	MS/SnO ₂	25 (RT)	1.15 (RT)	0.2/650 (RT)	23
$\text{Li}_{6.5}\text{La}_3\text{Zr}_{1.5}\text{Ta}_{0.5}\text{O}_{12}$	Li-Na Eutectic Interlayer	54.01 (RT) 18.98 (60 °C)	1.1 (RT) 2.1 (60 °C)	0.05/3500 (RT)	24
				0.1/3000 (RT)	
$\text{Li}_{6.4}\text{La}_3\text{Zr}_{1.4}\text{Ta}_{0.6}\text{O}_{12}$	MS/ITO	32 (30 °C)	1.05 (30 °C)	0.2/800 (30 °C)	25
$\text{Li}_{6.4}\text{La}_3\text{Zr}_{1.4}\text{Ta}_{0.6}\text{O}_{12}$	Flame Vapor Deposition	50 (60 °C)	0.6 (60 °C)	0.1/450 (60 °C)	26
$\text{Li}_{6.75}\text{La}_3\text{Zr}_{1.75}\text{Nb}_{0.25}\text{O}_{12}$	Sulfur Layer	160	N/A	0.2/1100	27

Li _{6.4} Ga _{0.2} La ₃ Zr ₂ O ₁₂	MS/Cu	29	0.4	0.1/135 0.2/140	28
Li _{6.5} La ₃ Zr _{1.5} Ta _{0.5} O ₁₂	H ₃ PO ₄	7 (25 °C)	0.8 (25 °C)	0.1/1600 (25 °C) 0.5/450 (25 °C)	29
Li _{6.4} Ga _{0.2} La ₃ Zr ₂ O ₁₂	MS/3D Zn layer	1.9 (RT)	2 (RT)	0.1/1000 (RT) 0.5/300 (RT)	30
Li _{6.4} La ₃ Zr _{1.4} Ta _{0.6} O ₁₂	Graphite foils	15 (RT)	0.8 (RT)	0.1/1600 (RT)	31
Li _{6.4} La ₃ Zr _{1.4} Ta _{0.6} O ₁₂	LiTFSI-FEC-SN	N/A	0.2 (RT)	0.2/150 (RT)	32
Al-Li _{6.75} La _{2.75} Ca _{0.25} Zr _{1.5} Ta _{0.5} O ₁₂	Liquid Phase Process/ Li ₂ SiO ₃	44 (25 °C)	0.5 (25 °C)	0.1/600 (25 °C)	33
Li _{6.4} La ₃ Zr _{1.4} Ta _{0.6} O ₁₂	Thermal evaporation deposition /LiF	12.7/(RT)	0.75 (RT)	0.2/1500 (RT) 0.4/300 (RT)	34
Li _{1.4} Al _{0.4} Ti _{1.6} (PO ₄) ₃	MS/ZnO	176.5 (RT)	N/A	0.05/2000 (RT) 0.2/1000 (RT)	35
Li _{1.5} Al _{0.5} Ge _{0.5} P ₃ O ₁₂	MS/Ge	73.5 (RT)	N/A	0.3/200 (RT)	36
Li _{6.4} La ₃ Zr _{1.4} Ta _{0.6} O ₁₂	InCl ₃	10 (25 °C)	0.7 (25 °C)	0.2/4000 (25 °C) 0.45/1000 (25 °C)	37
Li _{6.75} La ₃ Zr _{1.75} Ta _{0.25} O ₁₂	Spin coating/MgF ₂	25 (25 °C)	0.65 (25 °C)	0.3/1000 (25 °C)	38
Li _{1.5} Al _{0.5} Ge _{0.5} P ₃ O ₁₂	Ionic Liquid	5 (RT)	2 (RT)	0.1/1500 (RT) 1/500 (RT)	39
Li _{6.4} La ₃ Zr _{1.4} Ta _{0.6} O ₁₂	Li ₃ N/Fe	4 (60 °C)	3 (60 °C)	0.1/3000 (60 °C)	40
Li _{6.4} La ₃ Zr _{1.4} Ta _{0.6} O ₁₂	Li-Si ₃ N ₄	1 (25 °C)	1.8 (25 °C)	0.4/1000 (25 °C)	41
Li _{6.4} La ₃ Zr _{1.4} Ta _{0.6} O ₁₂	Li _x SiO _y	3 (30 °C)	1.3 (30 °C)	0.1/999 (30 °C)	42
Li _{1.5} Al _{0.5} Ge _{1.5} (PO ₄) ₃	MS/ZnF ₂	420 (25 °C)	2 (25 °C)	0.1/1000 (25 °C) 0.2/400 (25 °C)	43
Li ₇ La ₃ Zr ₂ O ₁₂	Li ₂ O	30 (30 °C)	1.3 (30 °C)	0.3/2500 (30 °C)	44
Li _{6.4} La ₃ Zr _{1.4} Ta _{0.6} O ₁₂	PAA	54.5	1.2	0.2/1000 (25 °C) 0.5/400 (25 °C)	45
Li _{6.4} La ₃ Zr _{1.4} Ta _{0.6} O ₁₂	Hard carbon layer	4.7 (40 °C)	1.0 (40 °C)	0.2/600 (40 °C)	46
Li _{6.5} La ₃ Zr _{1.5} Nb _{0.5} O ₁₂	MS/LiPON	178 (30 °C)	0.62 (30 °C)	0.04/2000 (30 °C)	47
Li _{6.4} La ₃ Zr _{1.4} Ta _{0.6} O ₁₂	Flexible graphite layer	26.2 (RT)	N/A	0.3/900 (RT)	48
Li _{6.5} La ₃ Zr _{1.5} Ta _{0.5} O ₁₂	Mechanical polishing	28.15 (RT)	0.76 (RT)	0.1/1200 (RT) 0.2/400 (RT)	49
Li _{6.4} La ₃ Zr _{1.4} Ta _{0.6} O ₁₂	Li-Naph	131.8 (25 °C) 9.9 (65 °C)	1.7 (65 °C)	0.2/1200 (25 °C) 1.0/500 (65 °C)	50
Li _{6.4} La ₃ Zr _{1.4} Ta _{0.6} O ₁₂	Li-Li _{0.3} La _{0.5} TiO ₃	48 (RT)	0.4 (RT)	0.1/400 (RT)	51
Li _{6.5} La ₃ Zr _{1.5} Ta _{0.5} O ₁₂	MS/h-BN	18 (60 °C)	0.9 (60 °C)	0.5/200 (60 °C)	52
Li _{1.5} Al _{0.5} Ge _{1.5} P ₃ O ₁₂	Liquid electrolyte	1100 (25 °C)	N/A	0.1/1600 (25 °C) 0.5/200 (25 °C)	53
Li _{6.5} La ₃ Zr _{1.5} Nb _{0.5} O ₁₂	wet-chemistry	8.4 (25 °C)	1.0 (25 °C)	0.1/600 (25 °C)	54

fabrication/Al ₂ O ₃				0.3/1000 (25 °C)	
Li _{6.75} La ₃ Zr _{1.75} Ta _{0.25} O ₁₂	Li-MXene	5 (RT)	1.5 (RT)	0.3/600 (RT)	55
Li _{6.75} La ₃ Zr _{1.75} Ta _{0.25} O ₁₂	SnS ₂	47 (RT)	0.5 (RT)	0.1/1000 (RT) 0.2/1000 (RT)	56
Li ₇ La ₃ Zr ₂ O ₁₂	Sb	4.1 (RT)	0.64 (RT)	0.2/350 (RT)	
Li _{1.3} Al _{0.3} Ti _{1.7} (PO ₄) ₃	BN	375 (RT)	0.76 (RT)	0.05/1800 (RT) 0.2/1200 (RT)	57
Li _{6.4} La ₃ Zr _{1.4} Ta _{0.6} O ₁₂	Laser cleaning Li ₂ CO ₃	76.4 (30 °C)	N/A	0.1/200 (80 °C) 0.2/100 (80 °C)	52
Li _{6.5} La ₃ Zr _{1.5} Ta _{0.5} O ₁₂	Dip-coating/MgO	6 (25 °C)	1.2 (25 °C)	0.1/4000 (25 °C) 0.2/1200 (25 °C)	58
Li _{6.4} La ₃ Zr _{1.4} Ta _{0.6} O ₁₂	Ag/LiF	13.4 (25 °C)	0.75 (25 °C)	0.2/600 (25 °C) 0.5/130 (25 °C)	59
Li _{6.75} La ₃ Zr _{1.75} Ta _{0.25} O ₁₂	TVD/Carbon layer	9 (RT)	1.2 (RT)	0.1/1000 (RT) 0.2/1000 (RT)	60
Li _{6.4} La ₃ Zr _{1.4} Ta _{0.6} O ₁₂	Li ₃ PO ₄	13 (25 °C)	1.2 (25 °C)	0.1/1000 (25 °C) 0.3/200 (25 °C) 0.4/200 (25 °C)	61
Li _{6.4} La ₃ Zr _{1.4} Ta _{0.6} O ₁₂	Li-LiNO ₃	1.73 (RT)	1.4 (RT)	0.3/4500 (RT) 0.5/500 (RT)	This work
	Pure Li	527.5 (RT)	0.1 (RT)	0.1/1 (RT)	

Table S2. Cathode materials, voltage windows, rate/cycles, and discharge capacities of the reported full batteries using garnet solid-state electrolytes with different interfacial layers.

Interfacial layer	Cathode	Voltage Window/V	Rate/C	Discharge Capacity/mAh g ⁻¹ /Cycle Number
Vapor Deposition Method/Al	LiFePO ₄	2.0-4.5	0.1	132/100 (20 °C)
PECVD/Li ₃ N	LiFePO ₄	2.5-4.0	0.05 0.1	143/100 (40 °C) 133/200 (40 °C)
ALD/Al ₂ O ₃	Li ₂ FeMn ₃ O ₈	3.5-5.3	0.1	103/50 (RT)
Li-C	LiFePO ₄	2.5-4.0	0.5	N/A/100 (RT)
Li ₃ N/Fe	LiFePO ₄	2.5-4.0	0.5	151/50 (60 °C)
Cu ₃ N	LiCoO ₂	3.2-4.2	0.2	125.3/300 (25 °C)
Sr	NCM811	2.7-4.3	0.2	192/100
MgO	NCM0.83	3.0-4.3	0.2	194.3/150 (25 °C)
Porous hard carbon	LiFePO ₄	2.8-3.8	0.2	154.4/150 (25 °C)
SnS ₂	LiFePO ₄	2.0-4.2	0.1	153.2/100
Sb	V ₂ O ₅	2.0-3.8	0.05	274/10 (RT)
Flexible graphite layer	LiFePO ₄	2.5-4.2	0.1	149.4/350
Laser cleaning Li ₂ CO ₃	LiFePO ₄	2.8-3.8	0.1	149.3/100 (40 °C)
Si ₃ N ₄	LiFePO ₄	2.2-4.2	1	152/100 (60 °C)
MgF ₂	LiFePO ₄	2.5-4.2	0.1	158.2/100 (25 °C)
Ga	LiFePO ₄	2.5-3.8	0.15 mA cm ⁻²	130/440 (60 °C)
h-BN	LiFePO ₄	2.8-4.0	0.2	130/100 (60 °C)
α-MoO ₃	LiFePO ₄	2.2-4.2	0.5	135/200 (RT)
ZnF ₂	LiFePO ₄	2.5-4.2	0.1	154/40 (25 °C)
InCl ₃	LiFePO ₄	2.8-3.8	0.5	127.4/475
Mechanical polishing	LiFePO ₄	2.5-4.0	0.2	138.6/80 (RT)
BN	LiFePO ₄	2.5-4.0	0.5	150.9/500 (RT)
LiPON	LiFePO ₄	2.5-4.0	0.2	138.1/150 (30 °C)

ZnO/rGO	LiFePO ₄	2.5-4.0	0.5	131.6/100 (30 °C)
Li _x SiO _y	LiFePO ₄	2.5-4.0	0.05 mA cm ⁻²	127.6/80 (30 °C)
Li-Naph	LiFePO ₄	2.4-3.8	0.2	142.5/200(65 °C)
Li-MXene anode	LiFePO ₄	2.5-4.2	0.5	148/100 (25 °C)
Liquid electrolyte	LiFePO ₄	2.5-4.2	0.2	145.1/500 (25 °C)
3D porous Zn layer	NCM523	2.7-4.3	0.1	143.8/170 (RT)
PAA	LiFePO ₄	2.5-4.0	0.2 0.5	130.2/300 (25 °C) 125/200 (25 °C)
Ta ₂ O ₅	LiFePO ₄	2.5-4.0	0.2	153.1/100 (25 °C)
COF	LiFePO ₄	2.7-3.8	0.5	130/260 (RT)
C Reduction	LiFePO ₄	2.5-3.8 2.5-4.2	0.1 0.1	143/50 (65 °C) N/A/10 (65 °C)
Carbon layer	LiCoO ₂	3.0-4.3	0.5	100 (RT)
Li ₃ PO ₄	LiCoO ₂	3.0-4.3	0.1	130.0/150 (30 °C)
Li-LiNO ₃	LiFePO ₄	2.5-4.0	1	148.5/500 (RT)
	NCM811	2.7-4.3	0.2	178.8/115 (RT)
Pure Li	LiFePO ₄	2.5-4.0	0.1	0/0 (RT)

Reference

1. K. K. Fu, Y. Gong, B. Liu, Y. Zhu, S. Xu, Y. Yao, W. Luo, C. Wang, S. D. Lacey, J. Dai, Y. Chen, Y. Mo, E. Wachsman and L. Hu, *Sci Adv*, 2017, **3**, e1601659.
2. C. Wang, Y. Gong, B. Liu, K. Fu, Y. Yao, E. Hitz, Y. Li, J. Dai, S. Xu, W. Luo, E. D. Wachsman and L. Hu, *Nano Lett*, 2017, **17**, 565-571.
3. C. L. Tsai, V. Roddatis, C. V. Chandran, Q. Ma, S. Uhlenbruck, M. Bram, P. Heitjans and O. Guillon, *ACS Appl Mater Interfaces*, 2016, **8**, 10617-10626.
4. W. Luo, Y. Gong, Y. Zhu, K. K. Fu, J. Dai, S. D. Lacey, C. Wang, B. Liu, X. Han, Y. Mo, E. D. Wachsman and L. Hu, *J Am Chem Soc*, 2016, **138**, 12258-12262.
5. H. Xu, Y. Li, A. Zhou, N. Wu, S. Xin, Z. Li and J. B. Goodenough, *Nano Lett*, 2018, **18**, 7414-7418.
6. X. Han, Y. Gong, K. Fu, X. He, G. T. Hitz, J. Dai, A. Pearse, B. Liu, H. Wang, G. Rubloff, Y. Mo, V. Thangadurai, E. D. Wachsman and L. Hu, *NATURE MATERIALS* (47.656), 2017, **16**, 572-579.
7. J. Duan, W. Wu, A. M. Nolan, T. Wang, J. Wen, C. Hu, Y. Mo, W. Luo and Y. Huang, *Adv Mater*, 2019, **31**, e1807243.
8. H. Y. Huo, Y. Chen, N. Zhao, X. T. Lin, J. Luo, X. F. Yang, Y. L. Liu, X. X. Guo and X. L. Sun, *Nano Energy* (19.069), 2019, **61**, 119-125.
9. H. Y. Huo, Y. Chen, R. Y. Li, N. Zhao, J. Luo, J. G. P. da Silva, R. Mucke, P. Kaghazchi, X. X. Guo and X. L. Sun, *Energy & Environmental Science* (39.714), 2020, **13**, 127-134.
10. W. Luo, Y. Gong, Y. Zhu, Y. Li, Y. Yao, Y. Zhang, K. K. Fu, G. Pastel, C. F. Lin, Y. Mo, E. D. Wachsman and L. Hu, *Adv Mater*, 2017, **29**, 1606042.
11. Y. Lu, X. Huang, Y. Ruan, Q. Wang, R. Kun, J. Yang and Z. Wen, *Journal of Materials Chemistry A* (14.511), 2018, **6**, 18853-18858.
12. Y. Li, X. Chen, A. Dolocan, Z. Cui, S. Xin, L. Xue, H. Xu, K. Park and J. B. Goodenough, *J Am Chem Soc*, 2018, **140**, 6448-6455.
13. K. K. Fu, Y. Gong, Z. Fu, H. Xie, Y. Yao, B. Liu, M. Carter, E. Wachsman and L. Hu, *Angew Chem Int Ed Engl*, 2017, **56**, 14942-14947.
14. M. H. He, Z. H. Cui, C. Chen, Y. Q. Li and X. X. Guo, *Journal of Materials Chemistry A* (14.511), 2018, **6**, 11463-11470.
15. W. L. Feng, X. L. Dong, P. L. Li, Y. G. Wang and Y. Y. Xia, *JOURNAL OF POWER SOURCES* (9.794), 2019, **419**, 91-98.
16. W. L. Feng, X. L. Dong, Z. Z. Lai, X. Y. Zhang, Y. G. Wang, C. X. Wang, J. Y. Luo and Y. Y. Xia, *ACS Energy Letters* (23.991), 2019, **4**, 1725-1731.
17. W. D. Zhou, Y. Zhu, N. Grundish, S. Xin, S. F. Wang, Y. You, N. Wu, J. Gao, Z. M. Cui, Y. T. Li and J. B. Goodenough, *Nano Energy* (19.069), 2018, **53**, 926-931.
18. Y. J. Shao, H. C. Wang, Z. L. Gong, D. W. Wang, B. Z. Zheng, J. P. Zhu, Y. X. Lu, Y. S. Hu, X. X. Guo, H. Li, X. J. Huang, Y. Yang, C. W. Nan and L. Q. Chen, *ACS Energy Letters* (23.991), 2018, **3**, 1212-1218.
19. J. M. Fu, P. F. Yu, N. Zhang, G. X. Ren, S. Zheng, W. C. Huang, X. H. Long, H. Li and X. S. Liu, *Energy & Environmental Science* (39.714), 2019, **12**, 1404-1412.
20. Y. Huang, B. Chen, J. Duan, F. Yang, T. Wang, Z. Wang, W. Yang, C. Hu, W. Luo and Y. Huang, *Angewandte Chemie International Edition*, 2020, **59**, 3699-3704.
21. J. Meng, Y. Zhang, X. Zhou, M. Lei and C. Li, *Nat Commun*, 2020, **11**, 3716.

22. J. Wen, Y. Huang, J. Duan, Y. Wu, W. Luo, L. Zhou, C. Hu, L. Huang, X. Zheng, W. Yang, Z. Wen and Y. Huang, *ACS Nano* (18.027), 2019, **13**, 14549-14556.
23. Y. Chen, M. H. He, N. Zhao, J. M. Fu, H. Y. Huo, T. Zhang, Y. Q. Li, F. F. Xu and X. X. Guo, *JOURNAL OF POWER SOURCES* (9.794), 2019, **420**, 15-21.
24. Y. Zhang, J. W. Meng, K. Y. Chen, H. Wu, J. L. Hu and C. L. Li, *ACS Energy Letters* (23.991), 2020, **5**, 1167-1176.
25. J. Lou, G. Wang, Y. Xia, C. Liang, H. Huang, Y. Gan, X. Tao, J. Zhang and W. Zhang, *JOURNAL OF POWER SOURCES* (9.794), 2020, **448**, 227440.
26. Y. Zhang, J. Meng, K. Chen, Q. Wu, X. Wu and C. Li, *ACS Appl Mater Interfaces*, 2020, **12**, 33729-33739.
27. S. Zheng, Z. Fu, D. J. Dai and W. M. Zhao, *CERAMICS INTERNATIONAL* (5.532), 2019, **45**, 11955-11962.
28. X. Xiang, S. Cao, F. Chen, Q. Shen and L. Zhang, *JOURNAL OF THE ELECTROCHEMICAL SOCIETY* (4.386), 2019, **166**, A3028-A3030.
29. Y. Ruan, Y. Lu, X. Huang, J. Su, C. Sun, J. Jin and Z. Wen, *Journal of Materials Chemistry A* (14.511), 2019, **7**, 14565-14574.
30. Z. Wan, K. Shi, Y. Huang, L. Yang, Q. Yun, L. Chen, F. Ren, F. Kang and Y.-B. He, *JOURNAL OF POWER SOURCES* (9.794), 2021, **505**, 230062.
31. J. X. Zhang, J. Li, H. Y. Zhai, G. J. Tan and X. F. Tang, *ACS Applied Energy Materials* (6.959), 2020, **3**, 6139-6145.
32. Z. H. Lu, J. Yu, J. X. Wu, M. B. Effat, S. C. T. Kwok, Y. Lyu, M. M. F. Yuen and F. Ciucci, *Energy Storage Materials* (20.831), 2019, **18**, 311-319.
33. N. C. Rosero-Navarro, R. Kajiura, R. Jalem, Y. Tateyama, A. Miura and K. Tadanaga, *ACS Applied Energy Materials* (6.959), 2020, **3**, 5533-5541.
34. S. Tang, G. Chen, F. Ren, H. Wang, W. Yang, C. Zheng, Z. Gong and Y. Yang, *Journal of Materials Chemistry A* (14.511), 2021, **9**, 3576-3583.
35. X. Hao, Q. Zhao, S. Su, S. Zhang, J. Ma, L. Shen, Q. Yu, L. Zhao, Y. Liu, F. Kang and Y. B. He, *Advanced Energy Materials* (29.698), 2019, **9**, 1901604.
36. Y. J. Liu, C. Li, B. J. Li, H. C. Song, Z. Cheng, M. R. Chen, P. He and H. S. Zhou, *Advanced Energy Materials* (29.698), 2018, **8**, 1702374.
37. J. Leng, H. Liang, H. Wang, Z. Xiao, S. Wang, Z. Zhang and Z. Tang, *Nano Energy* (19.069), 2022, **101**, 107603.
38. J. Jiang, Y. Ou, S. Lu, C. Shen, B. Li, X. Liu, Y. Jiang, B. Zhao and J. Zhang, *Energy Storage Materials* (20.831), 2022, **50**, 810-818.
39. S. Xiong, Y. Liu, P. Jankowski, Q. Liu, F. Nitze, K. Xie, J. Song and A. Matic, *ADVANCED FUNCTIONAL MATERIALS* (19.924), 2020, **30**, 2001444.
40. Y. Zhong, C. Cao, M. O. Tadé and Z. Shao, *ACS Applied Materials & Interfaces* (10.383), 2022, DOI: 10.1021/acsami.2c09801.
41. M. J. Du, Y. Sun, B. Liu, B. B. Chen, K. M. Liao, R. Ran, R. Cai, W. Zhou and Z. P. Shao, *ADVANCED FUNCTIONAL MATERIALS* (19.924), 2021, **31**, 2101556.
42. J. Zhang, C. Wang, M. Zheng, M. Ye, H. Zhai, J. Li, G. Tan, X. Tang and X. Sun, *Nano Energy* (19.069), 2022, **102**, 107672.
43. J. Yu, Q. Liu, X. Hu, S. Wang, J. Wu, B. Liang, C. Han, F. Kang and B. Li, *Energy Storage Materials* (20.831), 2022, **46**, 68-75.

44. Y.-N. Yang, C.-H. Cui, Z.-Q. Hou, Y.-Q. Li and T. Zhang, *Energy Storage Materials* (20.831), 2022, **52**, 1-9.
45. H. Huo, J. Gao, N. Zhao, D. Zhang, N. G. Holmes, X. Li, Y. Sun, J. Fu, R. Li, X. Guo and X. Sun, *Nature Communications* (17.694), 2021, **12**, 176.
46. L. Chen, J. Zhang, R.-A. Tong, J. Zhang, H. Wang, G. Shao and C.-A. Wang, *Small* (15.153), 2022, **18**, 2106142.
47. Y. Niu, Z. Yu, Y. Zhou, J. Tang, M. Li, Z. Zhuang, Y. Yang, X. Huang and B. Tian, *Nano Research* (10.269), 2022, **15**, 7180-7189.
48. C. Cui, Q. Ye, C. Zeng, S. Wang, X. Xu, T. Zhai and H. Li, *Energy Storage Materials* (20.831), 2022, **45**, 814-820.
49. Z. Qin, Y. Xie, X. Meng, D. Qian, C. Shan, D. Mao, G. He, Z. Zheng, L. Wan and Y. Huang, *CHEMICAL ENGINEERING JOURNAL* (16.744), 2022, **447**, 137538.
50. B.-Q. Xiong, S. Chen, X. Luo, Q. Nian, X. Zhan, C. Wang and X. Ren, *Advanced Science* (17.521), 2022, **9**, 2105924.
51. C. Cao, Y. Zhong, K. Chandula Wasalathilake, M. O. Tadé, X. Xu, H. Rabiee, M. Roknuzzaman, R. Rahman and Z. Shao, *Journal of Materials Chemistry A* (14.511), 2022, **10**, 2519-2527.
52. S. Rajendran, A. Pilli, O. Omolere, J. Kelber and L. M. R. Arava, *CHEMISTRY OF MATERIALS* (10.508), 2021, **33**, 3401-3412.
53. P. Jiang, J. Cao, B. Wei, G. Qian, S. Wang, Y. Shi, G. Du, X. Lu, C. Ouyang, F. Cao and X. Lu, *Energy Storage Materials* (20.831), 2022, **48**, 145-154.
54. S. Guo, Y. Li, B. Li, N. S. Grundish, A.-M. Cao, Y.-G. Sun, Y.-S. Xu, Y. Ji, Y. Qiao, Q. Zhang, F.-Q. Meng, Z.-H. Zhao, D. Wang, X. Zhang, L. Gu, X. Yu and L.-J. Wan, *Journal of the American Chemical Society* (16.383), 2022, **144**, 2179-2188.
55. J. Wen, L. Huang, Y. Huang, W. Luo, H. Huo, Z. Wang, X. Zheng, Z. Wen and Y. Huang, *Energy Storage Materials* (20.831), 2022, **45**, 934-940.
56. B. Zhao, W. Ma, B. Li, X. Hu, S. Lu, X. Liu, Y. Jiang and J. Zhang, *Nano Energy* (19.069), 2022, **91**, 106643.
57. L. Zhu, Y. Wang, Y. Wu, W. Feng, Z. Liu, W. Tang, X. Wang and Y. Xia, *ADVANCED FUNCTIONAL MATERIALS* (19.924), 2022, **32**, 2201136.
58. T.-T. Wu, S. Guo, B. Li, J.-Y. Li, H.-S. Zhang, P.-Z. Ma, X. Zhang, C.-Y. Shen, X.-H. Liu and A.-M. Cao, *ACS Applied Materials & Interfaces* (10.383), 2022, **14**, 32026-32034.
59. S. Lee, K.-s. Lee, S. Kim, K. Yoon, S. Han, M. H. Lee, Y. Ko, J. H. Noh, W. Kim and K. Kang, *Science Advances* (14.957), 2022, **8**, eabq0153.
60. W. Feng, X. Dong, X. Zhang, Z. Lai, P. Li, C. Wang, Y. Wang and Y. Xia, *Angew Chem Int Ed Engl*, 2020, **59**, 5346-5349.
61. Z. Bi, Q. Sun, M. Jia, M. Zuo, N. Zhao and X. Guo, *ADVANCED FUNCTIONAL MATERIALS* (19.924), 2022, **n/a**, 2208751.